JOURNAL OF SANDWICH STRUCTURES & MATERIALS

*Article*

*Journal of Sandwich Structures and Materials*
15(1) 92–109
© The Author(s) 2012
Reprints and permissions:
sagepub.co.uk/journalsPermissions.nav
DOI: 10.1177/1099636212454538
jsm.sagepub.com
SAGE

# Low-velocity perforation behavior of composite sandwich panels with aluminum foam core

**Zhibin Li, Zhijun Zheng and Jilin Yu**

**Abstract**

Perforation response and failure of sandwich panels with composite face sheets and aluminum foam core are investigated experimentally in this paper. Quasi-static perforation and low-velocity impact tests are carried out by using a material test system and a drop weight machine, respectively. The load-displacement response, energy absorption and energy-absorbing effectiveness of sandwich panels are obtained and compared for quasi-static and impact tests. Effects of some key parameters on the overall energy absorption behavior of the panels are explored, such as impact energy, face sheets and core thickness, core density and indenter nose shape.

**Keywords**

Sandwich panel, aluminum foam, perforation, energy absorption, energy-absorbing effectiveness factor

## Introduction

Sandwich panels with composite face sheets and foam core are widely used in lightweight constructions, especially in aerospace industries, due to their advantages over the conventional structural constructions, such as high specific strengths and stiffness and good weight saving [1]. An early study [2] has indicated that using composite materials instead of aluminum for the face sheets results in higher performance and lower weight. In the meanwhile, as a new multi-functional engineering material, aluminum foam has many useful properties, such as low

CAS Key Laboratory of Mechanical Behavior and Design of Materials, University of Science and Technology of China, China

**Corresponding author:**
Zhijun Zheng, CAS Key Laboratory of Mechanical Behavior and Design of Materials, University of Science and Technology of China, Hefei, Anhui 230026, P. R. China.
Email: zjzheng@ustc.edu.cn

density, high specific stiffness, good impact resistance, high energy absorption capacity, easy to manufacture into complex shape, good erosion resistance [3,4], so it is usually used as core material of sandwich panels. However, it has also been found that composite sandwich panels are susceptible to impact damage caused by runway debris, hailstones, dropped tools and so on [2]. The resulting impact damage to the sandwich panel ranges from face sheet indentation to complete perforation, with the strength and reliability of the structures dramatically affected. Unlike for their solid metallic counterparts, making predictions of the effects of low-velocity impact damage are difficult and are still relatively immature. Hence, the behavior of sandwich structures with aluminum foam core under low-velocity impact has received increasing attention.

Recently, a number of studies have shown that localized impact loading on a sandwich structure can result in the generation of local damage, which can lead to significant reductions in its load-carrying capacity [5]. Investigations have been carried out on sandwich panels with foam core under quasi-static and impact loadings to explore the perforation energy absorbing mechanisms, mostly on sandwich structures with polymeric foam cores [6–8]. Wen et al. [6] have analyzed marine sandwich construction and they have identified the major energy absorbing modes as fragmentation under the penetrator and global panel deformation. Mines et al. [7] conducted a series of quasi-static perforation tests and low-velocity impact tests on square panels based on polymer composite sandwich structures. They suggested that higher impact velocities tend to increase the energy absorption, which is attributed to an increase in the core crush stress and skin failure stress at high strain rates. More comprehensive and detailed summaries of previous experimental studies can be found in a thorough review article of the impact response of sandwich structures given by Abrate [8]. While polymeric foams have been applied for many years, metallic foams have gained a significant and growing interest for applications in sandwich structures currently, for the reason that in comparison with polymer foams they exhibit excellent recycling efficiency, high specific stiffness, good thermal conductivity and high melting point. Kiratisaevee and Cantwell [9] investigated the impact response of sandwich panels with ALPORAS® foam cores and fiber-reinforced thermoplastic or fiber-metal laminate (FML) face-sheets. Impact tests were conducted by using a drop hammer at velocities up to 3 m/s. The resistance of these sandwich panels was found to be rate sensitive over the full range of conditions examined. Ruan et al. [10] have experimentally investigated the mechanical response and energy absorption of sandwich panels subjected to quasi-static indentation, which consist of aluminum face sheets and ALPORAS® foam core. The effects of several parameters, such as face sheet thickness, core thickness, boundary conditions, adhesive and surface condition of face sheets on the mechanical response and energy absorption during indentation are identified. While most of the existing investigations into the impact responses of composite sandwich structures with metallic foam cores have focused on high-velocity impact [11–16], only minimal attention has been paid on quasi-static and low-velocity tests, and few detailed parametric studies have been reported yet.

In the present study, a series of perforation tests were conducted on the sandwich panels with an aluminum foam core and two composite face sheets, which were subjected to quasi-static loading and low-velocity impact. The perforation responses of the sandwich panels are investigated and the deformation and failure modes observed during perforation are described in detail. The mechanical properties and collapse mechanisms of aluminum foam sandwich panels are correlated to the physical and geometric properties of the face sheets and foam core, so the effects of face sheet thickness, core thickness and relative density, the projectile nose shapes, as well as the effect of impact energy on the energy absorption capacity of sandwich panels are analyzed.

## Experimental investigation

### *Specimens and material properties*

The face sheets of sandwich panels are made of woven-glass fabric laminates (BQ-L-Y-3K-1). This fabric was E-glass fiber 7628 cloth with the filament diameter of about 10 μm, and the matrix is a thermosetting phenolic resin. The face sheets have a fiber volume ratio of 0.60 and a density of 2.31 g/cm$^3$ and were comprised of 0°/90°/0° configuration with the fiber orientation directions parallel to the sides of the panel. The face sheets were provided readymade with three nominal thicknesses, namely 1.2, 1.5 and 2.0 mm. It should be noted that the surface of the laminates is covered by a layer of silver-colored twill glass fabrics, so the visual patterns are not the actual fiber orientations. Uniaxial tensile tests were carried out to obtain the stress–strain curves in accordance with Chinese Standard GB/T 228-2002. Both the 0° and the 90° directions of the face sheet woven E-glass have been tested. Figure 1(a) gives typical strain–stress curves for the face sheets of three different wall thicknesses and they are averaged from a number of repeated

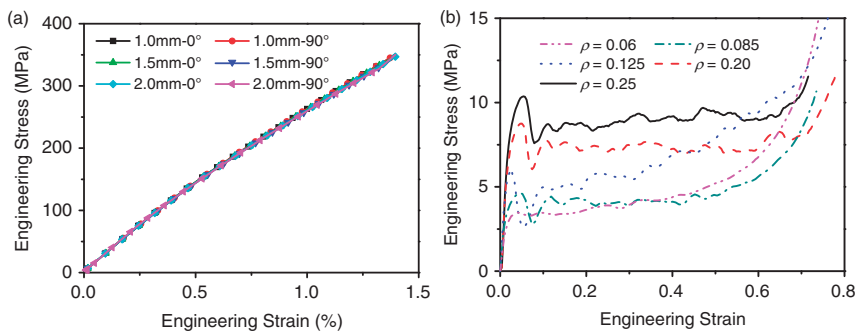


**Figure 1.** (a) Quasi-static tensile stress–strain curves of the face sheets with different thicknesses and (b) quasi-static uniaxial compression stress–strain curves of aluminum foams with different relative densities.

tests at strain rate of $10^{-3}$/s. It is noted that for both 0° and 90° directions, the samples have an ultimate stress of 330 MPa at a strain of 1.35% approximately before a sudden transverse failure of the specimen, with the elasticity modulus of about 25 GPa, regardless of the thickness.

The aluminum foam used as core material in the experiments is a closed-cell foam with the average cell size of approximately 3–5 mm, which is produced by liquid state processing with using $TiH_2$ as a foaming agent. Cylindrical specimens of which the diameter and height are both 30 mm were used in the uniaxial compression tests and the average values of mechanical properties of the foam core with five relative densities $\rho = \rho_f/\rho_s = 0.06$, 0.085, 0.125, 0.20 and 0.25, where $\rho_f$ is the density of foam and $\rho_s$ is the density of the cell-wall material, were assessed by means of compression tests performed and are shown in Figure 1(b). Four different thicknesses of aluminum foam cores, namely 10, 15, 20 and 30 mm, were used to investigate the effect of foam core thickness.

A commercial two-component impact-resistant adhesive SA102 was used to glue the face sheets and the foam core. Great attention has been given to achieve the perfect bonding between face sheets and foam core for a satisfactory structural performance, and the debonding effect will not be discussed in this study. The final sandwich panel specimen is a square plate $150 \times 150\,mm^2$ in dimensions. To ensure the repeatability of the tests, three specimens were tested for each selected case.

### *Quasi-static tests*

To determine the level to which dynamic processes should be considered in low-velocity impact testing, the sandwich panels were first tested under quasi-static loading for subsequent comparison with the impact loading cases. An MTS809 test system in the Engineering and Material Testing Center, USTC, was used to perform the quasi-static perforation. Specimens were fully clamped along all edges by using two steel frames with a span of $150 \times 150\,mm^2$, leaving an exposed square ($90 \times 90\,mm^2$) in the center. The main indenter is conical-nosed and two different indenters with an identical diameter of 38 mm are used for comparison in this study. One is a flat-ended indenter and the other is a hemispherical-nosed indenter. The geometry and dimensions of indenters are shown in Figure 2. A constant crosshead speed of 0.02 mm/s was applied to load the samples until full failure and the force-displacement histories were recorded.

### *Low-velocity impact tests*

Low-velocity impact tests were conducted on a drop weight machine. The support conditions as well as nose shape and sizes of the projectiles are identical to those used in the quasi-static tests. The specimens were impacted at various energy levels in order to achieve different damage levels. The impact mass was varied from approximately 3 to 24 kg and the drop height ranged between 51 mm and 1275 mm. An accelerometer was embedded inside the hammer just above the

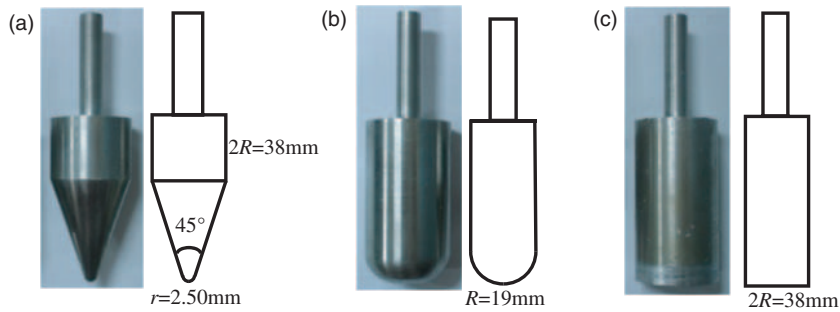


**Figure 2.** Geometry and dimensions of the indenters: (a) conical-nosed, (b) hemispherical-nosed and (c) flat-ended.

impactor tip to get the velocity and displacement history. For more details, the reader is referred to Reference [17].

An important issue in measuring the mechanical properties of foams is the effect of the specimen size, relative to the cell size. The size effect is also particularly important for foam core sandwich panels, as in some components the foam core may have dimensions of only a few cell diameters. As for sandwich beams with laminate skins and foam core, the size effect has already been experimentally demonstrated for shear failure of four-point bending [18]. In the current study, the ratio of the indenter diameter to the average cell size is about 10, thus no significant effect of cell size on perforation response will be noticed according to Andrews et al. [19]. The size effect can be avoided if the foam plate has at least eight cell diameters in thickness according to Reference [20]. However, the thin and stiff face sheets will give a better distribution of load throughout the area when subjected to loads, which would lead to a lower localized mean load and diminish the size effects. Moreover, in real sandwich components, the foam cores may just have limited cell diameters across the thickness of the panels despite the foam core is only about five cell diameters in thickness in this study.

## Experimental results

### *Load history*

For clarity, only one quasi-static load-displacement curve of specimens 2.0-15-1.5 (upper face-sheet thickness $H_{uf} = 2.0\,mm$, foam core thickness $H_c = 15\,mm$ and lower face-sheet thickness $H_{lf} = 1.5\,mm$) with a relative density of $\rho = 0.085$ from quasi-static perforation tests are shown in Figure 3. It demonstrates the following key features. The force first increases gradually before reaching the first peak, point A in Figure 3. This is a local indentation phase in which the conical-nosed indenter incrementally crushes the foam core and damages the upper face-sheet. The drop in load-displacement curve at point A in Figure 3 corresponds to tensile failure of the upper face-sheet. Subsequently, the panel continues to be loaded and the force

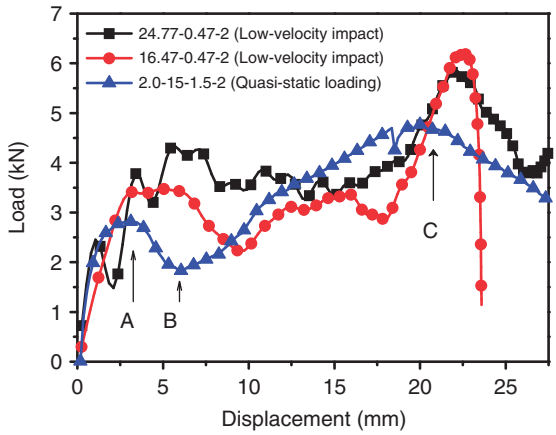


**Figure 3.** Force–displacement curves of sandwich specimens under conical indenter.

increases again to the second peak. This phase corresponds to the increase in the damage of the upper face-sheet, the crushing of the foam core and the penetrating of the sandwich panel by the indenter. Finally, the lower face-sheet fails at point C due to tensile tearing and the load drops to a level corresponding to the friction force as the conical-nosed indenter pierces the panel. All the panels with different thicknesses present similar behavior, but the deformation between upper and lower face sheet failure increases as the core thickness increases, and the magnitudes of the force are different for sandwich panels with different face-sheet thicknesses.

In order to make a comparison of the quasi-static and impact loading responses of sandwich panels, the force-displacement characteristics of identical panel configurations under different loading conditions are used. The details of the impact tests are listed in Table 1. Figure 3 illustrates a comparison between quasi-static and low-velocity impact perforations, in which the curves for specimens 24.77-0.47-2 and 16.47-0.47-2 are the impact loading responses. The specimens in dynamic tests are named as $<$impact mass level in kg$>-<$drop height level in m$>-<$repetition number$>$. It is found that increasing the impact velocity from $2 \times 10^{-5}$ m/s (quasi-static loading) to 3 m/s (low-velocity impact) produces similar deformation behavior and there is no large-scale difference in failure mechanisms for the panels tested under quasi-static and impact loading. For all quasi-static and impact tests, the load increases with the increasing of indenter/impactor displacement up to a first peak. At this point, the upper face-sheet fails and the load drops. After this, the load increases with foam core crushing until the lower face sheet fails and the specimen loses its load carrying ability. In particular, the energy conferred to the specimen until full perforation, which was calculated from the total area under the force-displacement curve up to point C in Figure 3, was found to be higher under impact condition than that in the static case. Thus, it has been found that the energy dissipated by the structures during perforation increases with the impact velocity.

**Table 1.** Experimental details of specimens loaded at various impact velocities and impact masses ($H_{uf} = 2.0$ mm; $H_c = 15$mm; $H_{lf} = 1.5$ mm; $\rho = 0.085$)

| Specimen (kg-m-#) | Impact mass (kg) | Drop height (mm) | Impact velocity (m/s) | $E_i$ (J) | $E_f$ or $E_m$ (J) | $\Psi$ | Deformation pattern |
|---|---|---|---|---|---|---|---|
| 12.41-0.05-1 | 12.405 | 54 | 0.98 | 6.56 | 5.96 | 0.032 | Upper face-sheet indent |
| 12.41-0.05-2 | 12.405 | 54 | 0.96 | 6.56 | 5.72 | 0.030 | Upper face-sheet indent |
| 12.41-0.21-1 | 12.405 | 205 | 1.87 | 24.92 | 21.69 | 0.12 | Foam core crushing |
| 12.41-0.21-2 | 12.405 | 205 | 1.95 | 24.92 | 23.59 | 0.13 | Foam core crushing |
| 12.41-0.47-1 | 12.405 | 465 | 2.92 | 56.53 | 52.88 | 0.28 | Foam core crushing |
| 12.41-0.47-4 | 12.405 | 465 | 2.96 | 56.53 | 54.34 | 0.29 | Foam core crushing |
| 12.41-0.82-1 | 12.405 | 816 | 3.85 | 99.20 | 81.94 | 0.44 | Full perforation |
| 12.41-0.82-2 | 12.405 | 816 | 3.90 | 99.20 | 78.77 | 0.42 | Full perforation |
| 12.41-1.28-1 | 12.405 | 1275 | 4.92 | 155.0 | 74.95 | 0.40 | Full perforation |
| 12.41-1.28-2 | 12.405 | 1275 | 4.78 | 155.0 | 86.54 | 0.46 | Full perforation |
| 3.38-0.47-1 | 3.383 | 465 | 2.90 | 15.42 | 14.23 | 0.076 | Upper face sheet failure |
| 3.38-0.47-2 | 3.383 | 465 | 2.78 | 15.42 | 13.07 | 0.070 | Upper face sheet failure |
| 6.27-0.47-1 | 6.271 | 465 | 2.82 | 28.58 | 24.93 | 0.13 | Foam core crushing |
| 6.27-0.47-3 | 6.271 | 465 | 2.85 | 28.58 | 25.47 | 0.14 | Foam core crushing |
| 16.47-0.47-1 | 16.472 | 465 | 2.84 | 75.06 | 67.66 | 0.36 | Lower face sheet failure |
| 16.47-0.47-2 | 16.472 | 465 | 2.77 | 75.06 | 68.64 | 0.37 | Lower face sheet failure |
| 24.77-0.47-2 | 24.773 | 465 | 2.97 | 112.89 | 74.80 | 0.40 | Full perforation |
| 24.77-0.47-3 | 24.773 | 465 | 2.96 | 112.89 | 80.11 | 0.43 | Full perforation |

## *Deformation of face-sheet and core*

The bending responses of sandwich panels tested under four-point bending configuration have been reported in a number of papers. Ashby et al. [4] have identified the competing collapse modes for sandwich beams with metallic face sheets and cores as face yielding, core shearing and indentation. In this study, similar failure patterns of aluminum foam core and composite face sheet sandwich panels are observed. Since the transverse deflections are small, membrane effects were neglected. Localized deformation in the upper face-sheet was observed from the beginning of each test. All top face-sheets cracked in a circular manner that corresponded to the striker diameter and tore into several pieces during tests, as can be seen in Figure 4(a), which resulted in the force drop from point A in Figure 3.

Figure 4(b) and (c) are the photographs of two different perforation damage patterns for the lower face-sheets. Damage mode-I in Figure 4(b) was observed in most sandwich panels that have a large area of lower face-sheet deformation, while

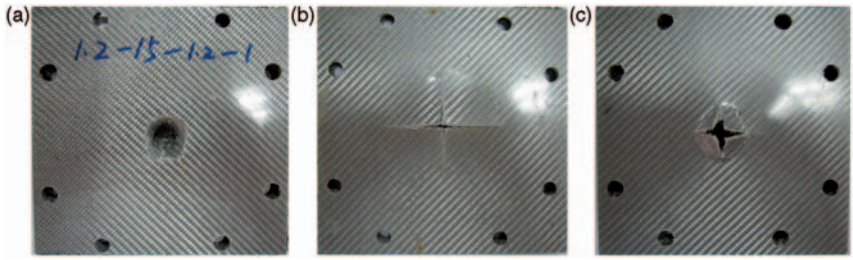


**Figure 4.** Photographs of post-test sandwich specimens under conical indenter: (a) upper face-sheet damage, (b) lower face-sheet damage mode-I and (c) lower face-sheet damage mode-II.

damage mode-II with localized damage was observed only a few times in sandwich panels with thick lower face-sheets. In both cases, the lower face-sheets tore in mutually perpendicular directions along the fiber 0/90° directions into four pieces in the central area under the indenter, and tensile failure in the lower face-sheets emanated from the center of the panel in four directions corresponding to the fiber directions of the woven face-sheets, resulting in a decrease of force after the second peak, point C in Figure 3. Then, full perforation occurred.

For specimens impacted at various energy levels, different damage levels were achieved. The sequence of failure up to perforation was obtained and shown in Figure 5. When the impact energy is too low, the impactor could only cause an indent in the upper face-sheet (Figure 5(a)). At an impact energy of 15 J, upper face-sheet failure occurs and the foam underneath the impactor nose is slightly crushed, as shown in Figure 5(b). As the impact energies increase, it becomes increasingly difficult to distinguish between force peaks of upper and lower face-sheet failure in Figure 3. So for intermediate energies (Figure 5(c) and (d)), the failure pattern corresponds to some intermediate condition between upper face-sheet failure and full perforation, such as foam core crushing. In Figure 5(c), the lower face sheet begins to deform, and the foam core directly underneath the indenter crushes, but no significant global deformation takes place in the panel. Figure 5(d) corresponds to the critical state of lower face-sheet failure while Figure 5(e) corresponds to full perforation, which means that the lower face-sheet is penetrated.

## *Energy-absorbing effectiveness*

In order to assist in the comparison of the efficiencies of different structures, extensive studies have been carried out on the energy-absorbing effectiveness factor $\Psi$ [21,22], which is defined as the quotient of the total energy which can be absorbed in a system to the maximum failure energy in a normal tensile specimen made from the same volume of materials. All the specimens are of the same geometry, the same materials and of the same constraints in this study, thus this dimensionless quantity can be adopted to compare the efficiencies of the

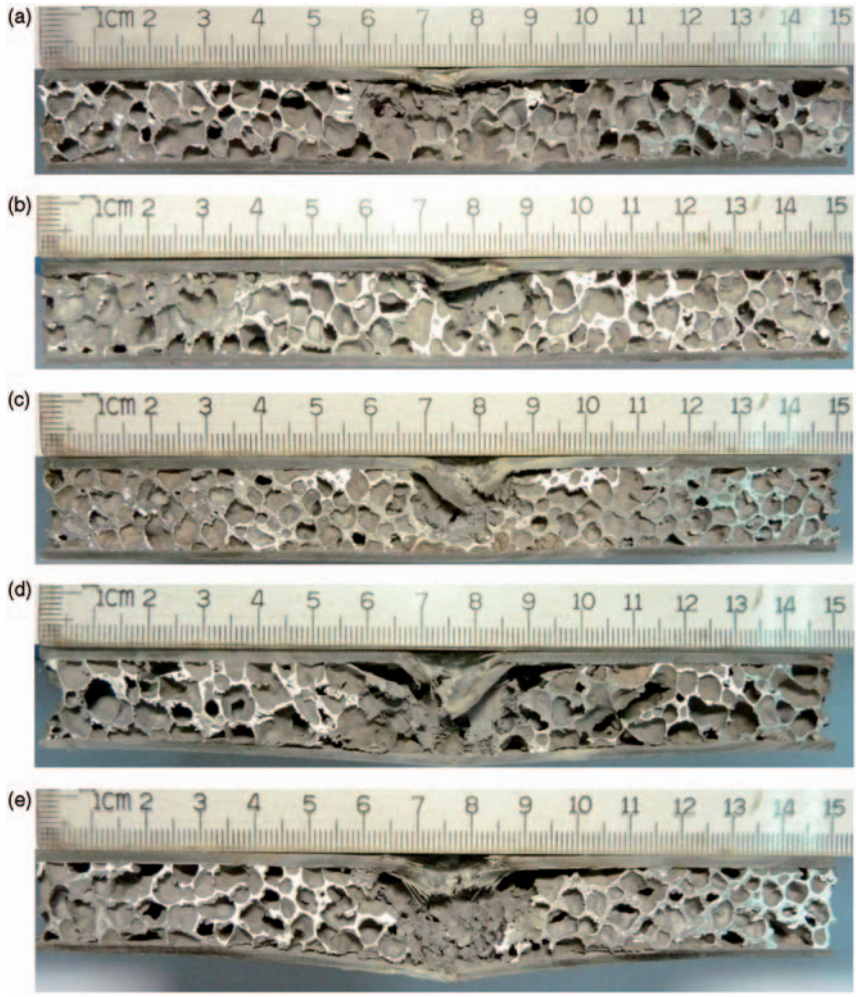


**Figure 5.** Cross-sections of sandwich specimens impacted by a conical indenter at different impact energy levels: (a) an indent in the upper face-sheet ($E_i = 6.56$ J), (b) upper face-sheet failure ($E_i = 15.42$ J), (c) foam core crushing ($E_i = 56.53$ J), (d) lower face-sheet failure ($E_i = 75.06$ J) and (e) full perforation ($E_i = 112.89$ J).

energy-absorbing structures. The energy-absorbing effectiveness factor $\Psi$ might be written in the form of

$$\Psi = \frac{\int_0^{\delta} F\mathrm{d}s}{V_{\mathrm{uf}} \int_0^{\varepsilon_r} \sigma_{\mathrm{f}}\mathrm{d}\varepsilon + V_{\mathrm{c}} \int_0^{\varepsilon_r} \sigma_{\mathrm{c}}\mathrm{d}\varepsilon + V_{\mathrm{lf}} \int_0^{\varepsilon_r} \sigma_{\mathrm{f}}\mathrm{d}\varepsilon} \tag{1}$$

where $F$ denotes the contact force, $s$ the displacement of the indenter/impactor, $\delta$ the maximum displacement of the indenter/impactor up to full perforation, $\varepsilon$ the

uniaxial tensile strain, $\varepsilon_r$ the uniaxial tensile engineering rupture strain of the composite face sheet (it is assumed that the maximum strain reached in the foam is equal to the uniaxial rupture strain of the face sheet material to simplify the analysis [21]), $\sigma_f$ the static strength of the upper and lower face sheet material, $\sigma_c$ the plateau crushing stress of the foam core, $V_c$ the volume of the foam core and $V_{uf}$ and $V_{lf}$ the volumes of the upper and lower face sheets, respectively. It deserves noting that the whole specimen was considered when calculating the volume.

For the clarity of the explanation of the energy absorption efficiencies, summaries of the energy-absorbing effectiveness factor are shown in Tables 1–4 and it will be discussed in detail in the next section.

## Discussion

From the results shown in the previous section, it is apparent that the impact mass, the face sheet thickness, the core thickness and density, as well as the projectile nose shape all have effects on the force-displacement curve and the energy absorption capacity of sandwich panels. These effects are discussed in detail as follows.

**Table 2.** Experimental details of specimens with different lower and upper face sheet thickness ($H_c = 15$ mm; $\rho = 0.085$; under conical-nosed indenter)

| Specimen | Peak force (kN) | | Energy absorption (J) | Mass of panels (kg) | Specific energy absorption (J/kg) | $\Psi$ | Rear face damage |
|---|---|---|---|---|---|---|---|
| | Point A | Point C | | | | | |
| 1.2-15-1.2-1 | 1.5 | 3.4 | 35 | 0.24 | 146 | 0.24 | Damage-I |
| 1.2-15-1.2-3 | 1.6 | 3.5 | 38 | 0.25 | 152 | 0.26 | Damage-I |
| 1.2-15-1.5-1 | 1.5 | 3.3 | 35 | 0.27 | 130 | 0.23 | Damage-I |
| 1.2-15-1.5-2 | 1.7 | 3.5 | 33 | 0.27 | 122 | 0.22 | Damage-I |
| 1.2-15-2.0-1 | 1.6 | 4.2 | 32 | 0.30 | 107 | 0.17 | Damage-II |
| 1.2-15-2.0-2 | 1.7 | 5.3 | 38 | 0.30 | 127 | 0.20 | Damage-II |
| 1.5-15-1.2-1 | 2.0 | 4.5 | 57 | 0.27 | 211 | 0.38 | Damage-I |
| 1.5-15-1.2-2 | 2.0 | 5.0 | 43 | 0.27 | 159 | 0.29 | Damage-I |
| 1.5-15-1.5-2 | 2.0 | 4.3 | 48 | 0.29 | 165 | 0.32 | Damage-II |
| 1.5-15-1.5-3 | 2.4 | 4.0 | 52 | 0.30 | 173 | 0.34 | Damage-I |
| 1.5-15-2.0-1 | 2.1 | 4.9 | 51 | 0.32 | 159 | 0.27 | Damage-II |
| 1.5-15-2.0-2 | 2.3 | 5.8 | 54 | 0.32 | 168 | 0.29 | Damage-I |
| 2.0-15-1.2-1 | 2.7 | 4.9 | 60 | 0.30 | 200 | 0.32 | Damage-I |
| 2.0-15-1.2-2 | 2.6 | 4.6 | 68 | 0.30 | 227 | 0.37 | Damage-I |
| 2.0-15-1.5-1 | 2.6 | 5.8 | 58 | 0.32 | 181 | 0.31 | Damage-I |
| 2.0-15-1.5-2 | 2.8 | 4.8 | 62 | 0.32 | 194 | 0.33 | Damage-I |
| 2.0-15-2.0-1 | 3.0 | 5.6 | 65 | 0.34 | 191 | 0.29 | Damage-I |
| 2.0-15-2.0-2 | 2.5 | 5.2 | 72 | 0.34 | 212 | 0.32 | Damage-I |

## Effect of impact energy

As it was found that the effects of "impact velocity" and "impact mass" make no essential differences in this study, thus the two aspects were combined together and generally considered as the effect of "impact energy". In this study, a number of

**Table 3.** Experimental details of specimens with different foam core thickness and relative density ($H_{uf} = 2.0$ mm; $H_{lf} = 1.5$ mm; under conical-nosed indenter)

| Specimen | Foam core | | Energy absorption (J) | Mass of panels (kg) | Specific energy absorption (J/kg) | Ψ |
|---|---|---|---|---|---|---|
| | Thickness (mm) | Relative density | | | | |
| 2.0-10-1.5-1 | 10 | 8.5% | 41 | 0.30 | 137 | 0.22 |
| 2.0-10-1.5-2 | 10 | 8.5% | 38 | 0.30 | 127 | 0.21 |
| 2.0-15-1.5-1 | 15 | 8.5% | 58 | 0.32 | 181 | 0.31 |
| 2.0-15-1.5-2 | 15 | 8.5% | 62 | 0.32 | 194 | 0.33 |
| 2.0-20-1.5-1 | 20 | 8.5% | 79 | 0.37 | 214 | 0.41 |
| 2.0-20-1.5-2 | 20 | 8.5% | 89 | 0.37 | 241 | 0.46 |
| 2.0-30-1.5-1 | 30 | 8.5% | 124 | 0.42 | 295 | 0.63 |
| 2.0-30-1.5-2 | 30 | 8.5% | 120 | 0.42 | 286 | 0.61 |
| 2.0-15-1.5-1(ρ1) | 15 | 6.4% | 42 | 0.30 | 140 | 0.23 |
| 2.0-15-1.5-2(ρ1) | 15 | 6.4% | 48 | 0.30 | 160 | 0.26 |
| 2.0-15-1.5-1(ρ2) | 15 | 12.6% | 78 | 0.35 | 223 | 0.40 |
| 2.0-15-1.5-2(ρ2) | 15 | 12.4% | 80 | 0.35 | 229 | 0.41 |
| 2.0-15-1.5-1(ρ3) | 15 | 19.6% | 104 | 0.39 | 267 | 0.54 |
| 2.0-15-1.5-2(ρ3) | 15 | 20.8% | 109 | 0.40 | 272 | 0.57 |
| 2.0-15-1.5-1(ρ4) | 15 | 24.7% | 124 | 0.42 | 295 | 0.65 |
| 2.0-15-1.5-2(ρ4) | 15 | 25.4% | 132 | 0.43 | 307 | 0.70 |

**Table 4.** Experimental details of specimens of identical configurations ($H_{uf} = 2.0$ mm; $H_c = 15$ mm; $H_{lf} = 1.2$ mm; $\rho = 0.085$) perforated by indenters of different nose shapes

| Specimen | Peak force (kN) | | Energy absorption (J) | Mass of panels (kg) | Specific energy absorption (J/kg) | Ψ |
|---|---|---|---|---|---|---|
| | Point A | Point C | | | | |
| 2.0-15-1.2-1 (conical-nosed) | 2.7 | 4.9 | 60 | 0.30 | 200 | 0.32 |
| 2.0-15-1.2-2 (conical-nosed) | 2.6 | 4.6 | 68 | 0.30 | 227 | 0.37 |
| 2.0-15-1.2-1 (flat-ended) | 11.8 | 8.6 | 100 | 0.30 | 334 | 0.54 |
| 2.0-15-1.2-2 (flat-ended) | 12.6 | 9.8 | 114 | 0.30 | 380 | 0.61 |
| 2.0-15-1.2-1 (hemispherical-nosed) | 7.7 | 9.2 | 137 | 0.30 | 457 | 0.74 |
| 2.0-15-1.2-2 (hemispherical-nosed) | 6.2 | 10.0 | 120 | 0.30 | 400 | 0.64 |

identical sandwich panels with $H_{uf} = 2.0\,mm$, $H_c = 15\,mm$, $H_{lf} = 1.5\,mm$ and $\rho = 0.085$ were impacted by the conical-nosed projectile at various impact energy levels. Five impact masses were considered, namely 3, 6, 12, 18 and 24 kg. Based on the acceleration signals recorded, the impact velocities and energy absorption were obtained. The ranges of impact mass, impact velocity and hence impact energy are listed in Table 1. Figure 6(a) gives the energy absorbed up to failure ($E_f$) or maximum load ($E_m$) with respect to the impact energy ($E_i$), while Figure 6(b) gives a failure map of sandwich panels tested at different impact energies. $E_f$ and $E_m$ were calculated from the area under the force-displacement curves and $E_i$ was calculated from the drop height. The failure load used in the calculation of $E_f$ corresponds to point C in Figure 3. Two horizontal lines are given in Figure 6(a), representing the static energy to upper face-sheet tearing (8 J) and lower face-sheet tearing, i.e. total perforation (60 J), which are calculated from the total area under the curves in Figure 3 up to point A and point C, respectively. Two curves corresponding to the energies associated to the upper and lower face-sheet failures, respectively, in static tests are also shown in Figure 6(b).

When the impact energy is low, the panel is only partially perforated and most impact energy is absorbed by the specimen, so the energy to maximum load or to failure is approximately equal to the impact energy. As the impact energy increases further, full perforation takes place and some kinetic energy may remain in the impact mass. Moreover, it can be seen from Figure 6(a) that when the impact energy is high enough, the energy absorbed by the specimen in the impact test is higher than that in the quasi-static case. However, this does not mean the energy required for the full failure of specimen is higher in dynamic cases. In Figure 6(b), all the data points of impact tests are in accordance with the two critical energy curves obtained in quasi-static tests. There is no evidence showing the strain rate effect, though further data are required to reach a solid conclusion. In general, no major differences in the gross failure modes from quasi-static to low-velocity impact loading conditions were discerned. Thus, the enhancement of energy

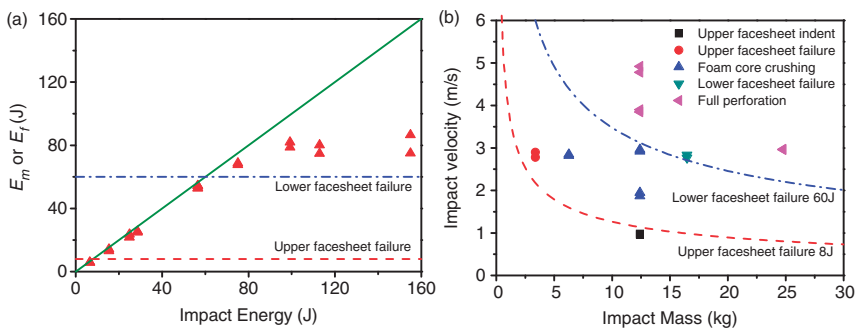


**Figure 6.** (a) $E_m$ or $E_f$ at different impact energy and (b) failure map for sandwich panels under conical indenter.

absorption under high impact energy can be attributed to the change in geometry of deformation and/or the inertia effect.

Table 1 shows the energy-absorbing effectiveness factors for different impact masses and velocities. It can be found that the energy-absorbing effectiveness factor gradually increases with the increasing of the impact energy. However, the dimensionless factor calculated by equation (1) reaches a nearly constant value of about 0.45 with a standard deviation of 0.023. This indicates that the sandwich panels cannot absorb more energy in low-velocity impact. And due to the brittleness of the composite face sheets, plastic deformation and failure concentrate at the localized area underneath the impactor and the material outside of the impact area remains inoperative, hence the values of energy-absorbing effectiveness factor $\Psi < 1$.

## *Effect of face-sheet thickness*

For all the sandwich panels tested under a conical-nosed indenter with core thickness of 15 mm and with different face sheet thicknesses, i.e. 1.2, 1.5 and 2.0 mm, the observed deformation and force-displacement curves demonstrate similar features. Figure 7 shows the effects of lower and upper face sheet thicknesses on the energy absorption in quasi-static perforations. The specifications of the panels and the results including the energy-absorbing effectiveness factors are listed in Table 2.

By comparing the results it is noted that the thickness of upper face sheet plays a very important role in the energy absorption of sandwich panels, while the thickness of lower face sheet does not show a clear effect on energy absorption. Moreover, it is interesting to note that the first peak force is lower than the second one even for the panels with a lower face sheet thicker than the upper face sheet. Table 2 and Figure 7 indicate that, for the range of thicknesses tested, the panels with thicker upper face sheets result in a higher force level and a higher energy absorption as well as a higher energy-absorbing effectiveness

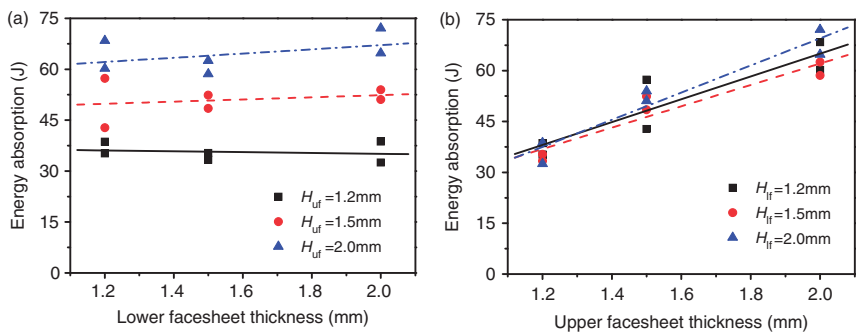


**Figure 7.** Effects of face sheet thickness under conical indenter: (a) lower face-sheet thickness $H_{lf}$ and (b) upper face-sheet thickness $H_{uf}$.

factor; while the total energy absorption are approximately equal for the panels with lower face sheets of different thicknesses. Moreover, the energy absorption is found to increase with the increasing of the upper face sheet thickness linearly, as can be seen in Figure 7. However, for sandwich panels with the same upper face sheet thickness and core thickness, thick lower face sheets result in lower specific energy absorption and a lower energy-absorbing effectiveness factor (Table 2). Besides, thinner lower face sheets usually lead to a larger deformation area of back faces and very limited global deformation is observed in sandwich panels with thick face sheets.

## *Effect of core thickness and core density*

A total of sixteen sandwich panels with four different core thicknesses and five different core densities were tested by using a conical-nosed indenter, as shown in Table 3. The effects of foam core thickness and relative density on energy absorption and energy-absorbing effectiveness factor are shown in Figure 8. The foam cores are crushed and densified as the indenter perforating the panels, and the core thickness will affect the displacement between upper face sheet failure and lower face sheet failure, i.e. the length between peak force A and C in Figure 3, hence the energy absorption and energy-absorbing effectiveness factor increase with the increasing of core thicknesses as shown in Figure 8(a).

As expected, sandwich panels with a denser core result in higher energy absorption. For the range of densities tested in this study, the energy absorption and energy-absorbing effectiveness factor are almost proportional to the core density. Moreover, the global bending of sandwich panels with denser cores seemed to be more obvious due to the higher resistant to deformation of the denser foam. These phenomena are because that higher density foam would give a better distribution of load throughout the area when subjected to load, which would lead to a lower localized mean load. Higher density foams also show a higher load carrying capacity and permit less deformation on their upper and lower face sheets.

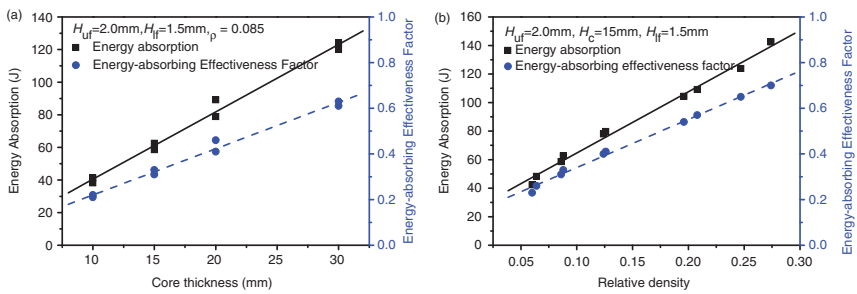


**Figure 8.** Effects of foam core configurations under conical indenter: (a) core thickness $H_c$ and (b) relative density $\rho$.

### *Effect of projectile nose shape*

Three different projectiles, i.e. conical-nosed, hemispherical-nosed and flat-ended, were used in this study. Six identical specimens were perforated by quasi-static loading. The specifications of the panels and the experimental results are listed in Table 4.

Figure 9 together with Figure 4 shows the upper and lower face-sheet failures of the panels after tests. To compare the resistance offered by the sandwich panels against the perforation of flat-ended, conical-nosed and hemispherical-nosed indenters, the force-displacement curves of specimens perforated by indenters with different nose shapes are plotted in Figure 10(a). By comparing with Figure 4, it is interesting to note that the flat-ended indenter punches through

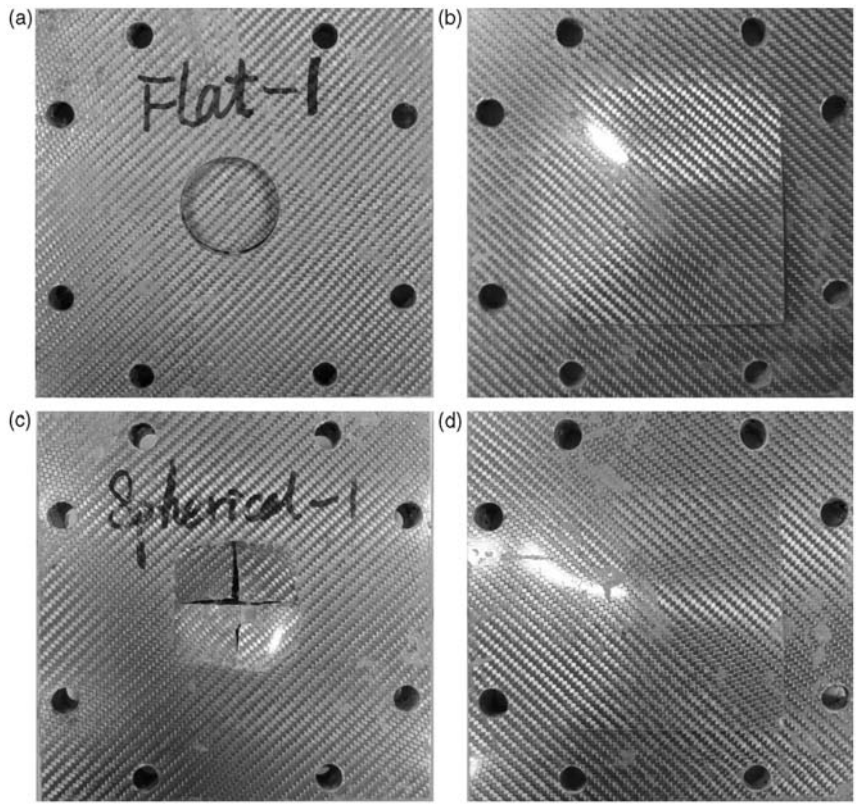


**Figure 9.** Photographs of post-test sandwich specimens: (a) upper face-sheet damage by flat-ended indenter, (b) lower face-sheet damage by flat-ended indenter, (c) upper face-sheet damage by hemispherical-nosed indenter and (d) lower face-sheet damage by hemispherical-nosed indenter.

the face sheet around the circumferential edge of the indenter while crushing the foam core underneath (Figure 9(a)) and results in a very large force (Figure 10(a)). A difference could be seen in the damage patterns of the upper face-sheet of the specimens loaded by hemispherical-nosed indenter, as shown in Figure 9(c). The hemispherical-nosed indenter produced cracks over a larger area in a square manner that is parallel and perpendicular to the fiber direction under the indenter. The face sheet tore into four pieces, as can be seen in Figure 9(c), and resulted in a relative high force in Figure 10(a). The hemispherical-nosed indenter and the flat-ended indenter both produced a larger area of fiber cracking than the conical-nosed indenter. Although the upper face sheet damage varied for each indenter, the lower face sheet damage was visually identical for flat-ended and hemispherical-nosed indenters, as shown in Figure 9(b) and (d). Unlike the specimens loaded by conical-nosed indenter, global bending was observed in the lower face sheets and finally, the lower face-sheets sheared along the edges of the frame of the fixture and experienced a much higher failure force. Although not a catastrophic failure mode, debonding between face sheets and foam core occurred when the bond strength is exceeded. However, the energy associated with debonding is very small and has negligible effect on the perforation behavior.

As shown in Figure 10(a), the force level was found to be highest for the flat-ended indenter, followed by the hemispherical-nosed indenter and then the conical-nosed indenter. However, significant reduction in the displacement of flat-ended indenter before lower face sheets failure was observed compared with the cases of the hemispherical-nosed indenter and the conical-nosed indenter. This could be a result of the varying damage mechanisms induced by different indenter shapes. It is interesting to note for the specimens loaded by the flat-ended indenter, the contact force between the indenter and specimen sharply increases to the first peak, then drops quickly, implying the sudden failure of the front face and the first peak force is much higher than the second one, which is different from the other two cases loaded by conical-nosed and hemispherical-nosed indenters.

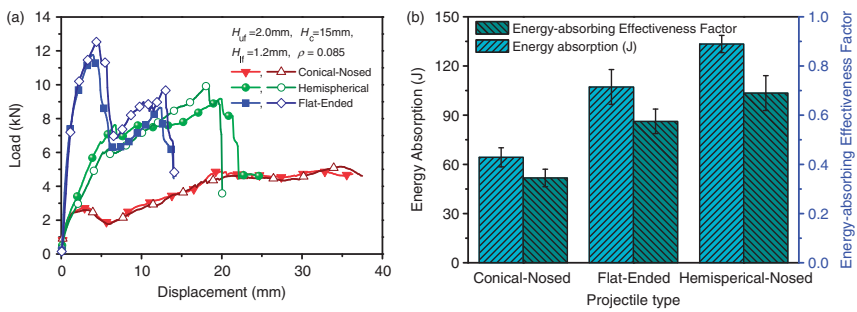


**Figure 10.** Effects of projectile nose shape on: (a) force–displacement curves and (b) energy absorption and energy-absorbing effectiveness (the error bars denote the standard deviations in replicate experiments).

It is clear that the energy required to perforate the sandwich panels and the energy-absorbing effectiveness factor depend on the indenter shape, as shown in Figure 10(b) (the error bars denote the standard deviations in replicate experiments). The sandwich panels perforated by the hemispherical-nosed indenter absorbed the highest energy, followed by the flat-ended indenter and then the conical-nosed indenter. Sandwich panels indented by the hemispherical-nosed indenter are more effective than structures indented by the other two indenters. The difference is attributed to the deformation and failure mechanism which varies with the indenter shape. More energy is required for the hemispherical-nosed indenter since it produces higher contact force and largest deformation area in the panel.

## Conclusions

Quasi-static perforation and low-velocity impact tests were carried out to study the mechanical response and energy absorption of sandwich panels with aluminum foam core and composite face sheets. The sandwich panels are perforated by three different indenters and the deformation and failure behavior of sandwich panels are explored. The load-displacement responses and energy absorption are recorded for quasi-static and impact tests. For all quasi-static and impact tests, the force increases with the indenter/impactor displacement up to a first peak force point associated to the failure of the upper face-sheet. Afterwards, the force drops to a valley and then increases with foam core crushing until the lower face sheet fails and the specimen loses its load carrying capacity.

The force-displacement curves and energy absorption of sandwich panels are affected by the impact mass and velocity, the face sheet thickness, the core thickness and density, as well as the projectile nose shape. It has been found that the energy-absorbing effectiveness factor increases with the increasing of the impact energy before it reaches a constant value. When the impact energy is high enough, the energy absorbed by the specimen in the impact test is higher than that in the quasi-static case. Moreover, thicker upper face-sheet, thicker or denser core are prone to absorbing higher energy and resulting in higher energy-absorbing effectiveness factors, while the thickness of lower face sheet does not show a clear effect on the energy absorption but will result in a lower energy-absorbing effectiveness factor. Three different indenters are used for comparison in this study: a conical-nosed, a hemispherical-nosed and a flat-ended indenter. The sandwich panels perforated by a hemispherical-nosed indenter absorb more energy than a flat-ended indenter as well as a conical-nosed indenter and so does the case with energy-absorbing effectiveness factor.

### Funding

The research reported herein is supported by the National Natural Science Foundation of China (Project no. 90916026), the Chinese Academy of Sciences (Grant no. KJCX2-EW-L03) and the National Key Technology R&D Program of China (2009BAG12A01-B02-2), which are gratefully acknowledged.

## References


1. Zenkert D. *An introduction to sandwich construction*. Sheffield: Engineering Materials Advisory Services Ltd., 1995.
2. Abrate S. *Impact on composite structures*. Cambridge: Cambridge University Press, 1998.
3. Gibson LJ and Ashby MF. *Cellular solids: structure and properties*, 2nd edn. Cambridge: Cambridge University Press, 1997.
4. Ashby MF, Evans AG, Fleck NA, et al. *Metal foams: a design guide*. Boston, MA: Butterworth Heinemann, 2000.
5. Hazizan MA and Cantwell WJ. The low velocity impact response of an aluminium honeycomb sandwich structure. *Compos Pt B* 2003; 34(8): 679–687.
6. Wen HM, Reddy TY, Reid SR, et al. Indentation, penetration and perforation of composite laminate and sandwich panels under quasi-static and projectile loading. *Key Eng Mater* 1997; 141–143(1): 501–552.
7. Mines RAW, Worrall CM and Gibson AG. Low velocity perforation behavior of polymer composite sandwich panels. *Int J Impact Eng* 1998; 21(10): 855–879.
8. Abrate S. Localized impact on sandwich structures with laminated facings. *Appl Mech Rev* 1997; 50(2): 69–82.
9. Kiratisaevee H and Cantwell WJ. Low-velocity impact response of high-performance aluminum foam sandwich structures. *J Reinf Plast Compos* 2005; 24(10): 1057–1072.
10. Ruan D, Lu G and Wong YC. Quasi-static indentation tests on aluminium foam sandwich panels. *Compos Struct* 2010; 92(9): 2039–2046.
11. Reyes Villanueva G and Cantwell WJ. The high velocity impact response of composite and FML-reinforced sandwich structures. *Compos Sci Technol* 2004; 64(1): 35–54.
12. Hanssen AG, Girard Y, Olovsson L, et al. A numerical model for bird strike of aluminium foam-based sandwich panels. *Int J Impact Eng* 2006; 32(7): 1127–1144.
13. Zhao H, Elnasri I and Girard Y. Perforation of aluminium foam core sandwich panels under impact loading-an experimental study. *Int J Impact Eng* 2007; 34(7): 1246–1257.
14. Hou W, Zhu F, Lu G, et al. Ballistic impact experiments of metallic sandwich panels with aluminium foam core. *Int J Impact Eng* 2010; 37(10): 1045–1055.
15. Buitrago BL, Santiuste C, Sánchez-Sáez S, et al. Modelling of composite sandwich structures with honeycomb core subjected to high-velocity impact. *Compos Struct* 2010; 92(9): 2090–2096.
16. Ivañez I, Santiuste C, Barbero E, et al. Numerical modelling of foam-cored sandwich plates under high-velocity impact. *Compos Struct* 2011; 93(9): 2392–2399.
17. Yu JL, Wang X, Wei ZG, et al. Deformation and failure mechanism of dynamically loaded sandwich beams with aluminum-foam core. *Int J Impact Eng* 2003; 28(3): 331–347.
18. Bažant ZP, Zhou Y, Daniel IM, et al. Size effect on strength of laminate-foam sandwich plates. *J Eng Mater Tech* 2006; 128(3): 366–374.
19. Andrews EW, Gioux G, Onck P, et al. Size effects in ductile cellular solids. Part II: experimental results. *Int J Mech Sci* 2001; 43(3): 701–713.
20. Tekoglu C, Gibson LJ, Pardoen T, et al. Size effects in foams: experiments and modeling. *Prog Mater Sci* 2011; 56(2): 109–138.
21. Jones N. Energy-absorbing effectiveness factor. *Int J Impact Eng* 2010; 37(6): 754–765.
22. Li ZB, Yu JL and Guo LW. Deformation and energy absorption of aluminum foam-filled tubes subjected to oblique loading. *Int J Mech Sci* 2012; 54(1): 48–56.